Defense Technical Information Center

Compilation Part Notice

ADP023772

TITLE: Chemical Oxygen-Iodine Laser Device Simulation Using the 3D, Unsteady Navier-Stokes Equations

DISTRIBUTION: Approved for public release, distribution unlimited

This paper is part of the following report:

TITLE: Proceedings of the HPCMP Users Group Conference 2007. High Performance Computing Modernization Program: A Bridge to Future Defense held 18-21 June 2007 in Pittsburgh, Pennsylvania

To order the complete compilation report, use: ADA488707

The component part is provided here to allow users access to individually authored sections of proceedings, annals, symposia, etc. However, the component should be considered within the context of the overall compilation report and not as a stand-alone technical report.

The following component part numbers comprise the compilation report:
ADP023728 thru ADP023803

Chemical Oxygen-Iodine Laser Device Simulation Using the 3D, Unsteady Navier-Stokes Equations

Timothy J. Madden

US Air Force Research Laboratory, Directed Energy Directorate (AFRL/DE), Kirtland AFB, NM
timothy.madden@kirtland.af.mil

Abstract

The time-dependent, chemically reacting, viscous fluid dynamics within the chemical oxygen-iodine laser (COIL) flowfield are simulated using the unsteady, laminar, multi-component Navier-Stokes equations. The solutions of these equations are generated within simulations of COIL hardware at standard operating conditions; conditions predicted in previous simulations to be unsteady. These current simulations ascertain the effect of the flow unsteadiness upon the laser gain through Doppler broadening of the spectral lineshape induced by the bulk movement of the gas. The results from the simulations demonstrate that the presence of bulk flow rotation associated with the unsteady vortex generation influences the temperature determined from the resulting lineshapes; this result has direct implications for experiments where spectroscopically measured lineshapes are utilized to determine flow temperatures. Additional simulations are used to test varying fidelity within the COIL finite-rate chemistry mechanism in the presence of the flow unsteadiness and H_2O vapor condensation. The same unsteady, laminar, multi-component Navier-Stokes simulation methodology is applied to new COIL mixing nozzle concepts with the goal of utilizing the unsteadiness flow to improve device performance. Experimental planar laser induced iodine fluorescence data for these nozzle concepts are directly compared to simulation data in a newly developed methodology for COIL model validation.

1. Introduction

Chemical lasers are complex devices that couple two-phase chemistry, fluid dynamics, and optics to generate coherent radiation capable of projecting high energy fluxes for very large distances at the speed of light. Given the complexity of the interactions between the various physical processes, simulation of chemical lasers presents an obvious opportunity for the application of high performance computing to facilitate the understanding and optimization of these devices. The work presented here illustrates how high performance computing is used to achieve an increased understanding of the physics underlying COILs and improve their operation. Computational fluid dynamic (CFD) simulations for the chemically reacting COIL flowfield are executed concomitant with achieving these goals.

2. Problem and Methodology

Chemical lasers generally operate on a series of exothermic, gas phase chemical reactions that create a population inversion, or non-Boltzmann energy distribution, within the energy states of the products of reactions. As these products equilibrate towards a Boltzmann distribution of energy states, photons are emitted via spontaneous emission. If an energetically excited species A^* emits a photon of energy $h\nu$ during the equilibration process, then this photon may collide with another excited species A^* causing it to release another photon with equal energy in the same direction of propagation as the first photon. This can be described as:

$$A^* \rightarrow A + h\nu$$
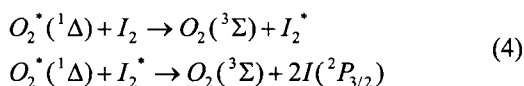$$h\nu + A^* \rightarrow A + 2h\nu \qquad (1)$$
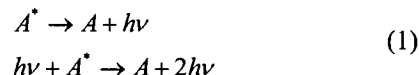
As the number of photons increases, a wave builds within the gas which when directed by mirrors that transmit a fraction of the photons and with each reflection of the waves, becomes a laser. As the wave builds within the gas, the increase in the number of photons or the wave intensity per given unit distance leads to the concept of gain in lasers. Gain is a key performance parameter in chemical lasers and is frequently referred to in this work. COIL generates the lasing species A^* via a complex series of chemical reactions, both liquid and gas phase. The first phase occurs in liquid, and generates the 'fuel' via the reaction:

$$Cl_2 + 2HO_2^- \rightarrow O_2^*(^1\Delta) + H_2O_2 + 2Cl \qquad (2)$$
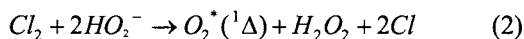
The electronically excited singlet-delta state of oxygen diffuses out of the liquid and is picked up by a carrier gas, usually He. COILs use $O_2(^1\Delta)$ collisions with ground state I atoms, $I(^2P_{3/2})$, to efficiently generate the lasing species $I^*(^2P_{1/2})$ via the energy transfer process:

$$O_2^*(^1\Delta) + I(^2P_{3/2}) \rightarrow O_2(^3\Sigma) + I^*(^2P_{1/2}) \qquad (3)$$
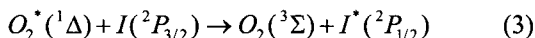
This reaction is more efficient at producing $I^*(^2P_{1/2})$ than any other known process, hence the reason a more direct reaction path to $I^*(^2P_{1/2})$ is not used. An additional reactive process occurs in COIL where $O_2^*(^1\Delta)$ dissociates molecular iodine, I_2, to generate the ground state I atoms, $I(^2P_{3/2})$. This multi-step energy transfer/reactive process occurs through the following reactions:

$$\begin{aligned} O_2^*(^1\Delta) + I_2 &\rightarrow O_2(^3\Sigma) + I_2^* \\ O_2^*(^1\Delta) + I_2^* &\rightarrow O_2(^3\Sigma) + 2I(^2P_{3/2}) \end{aligned} \qquad (4)$$

The exact state(s) of I_2 that I_2^* represents, is still somewhat of a point of contention amongst researchers at this time due to the considerable difficultly in constructing experiments to clearly identify and track multiple vibrational and electronic excited states. Because of the indeterminate nature of the I_2^* state(s) and the number of potential intermediate energy transfer processes involved, mathematical constructs are used to describe equation[4] but the construct is fitted to experimental measurements of the overall rate of dissociation of I_2.

The gas flows within COILs can be generally described as the flow of particles of different chemical composition with collisional interactions occurring between the particles and between the particles and the photons within the radiation field. Mathematically, this flow of particles is treated as a continuum and is approximated by the Navier-Stokes continuity equations for mass, momentum, and energy. In integral form, these equations are given by:

$$\frac{\partial}{\partial t} \iiint_{vol} \langle Q \rangle dvol + \oiint_A (\vec{F} - \vec{F}_v) \cdot \hat{n} dA$$
$$= \iiint_{vol} \langle S \rangle dvol \qquad (5)$$

where $\langle Q \rangle$ is the vector of the cell averaged conserved quantities of species density, momentum component, and pressure; $\vec{F}$ and $\vec{F}_v$ are the inviscid and viscous fluxes of the conserved quantities at the cell boundary, and $\langle S \rangle$ is the vector of cell averaged sources of the conserved quantities. Contained within these equations are descriptions for the rates of production and loss of reacting species, the production and absorption of photons, energy transfer within different modes in the molecules, molecular mixing, and temporal variation. Turbulence models are not employed due to the low Reynolds numbers, ~1,000, of the COIL flowfield. And as such, these simulations can be considered to be similar in nature to Direct Navier-Stokes simulations. The CFD code GASP from AeroSoft Inc., is employed to solve these equations for the simulations performed here.

Reacting flow, i.e., COIL, and non-reacting flow simulations of experiment hardware are performed in this work. The GASP COIL model utilizes separate species mass conservation equations for each of the chemically reacting components of the COIL flow in addition to the base conservation equations for momentum and energy. An effective binary diffusion model is used to describe concentration and pressure contributions to mass diffusion, an important process in the low density COIL flowfield. The COIL chemistry is described either using a 10 species, 22 reaction or a 13 species, 52 reaction finite-rate mechanism[1] that models the gas phase chemical kinetic processes generating the population inversion in atomic iodine necessary for laser oscillation. References providing additional details regarding the application of GASP to this problem may be found in Madden, et al.[2,3]

3. Results

We begin by updating the discussion of results regarding unsteady simulation of COIL. A three-dimensional (3D) GASP model for the COIL flowfield was executed in time accurate mode utilizing 1st-order accurate time integration and 3rd-order spatial accuracy at a physical time step of 1.0×10^{-9} sec for the simulation using the 10 species, 22 reaction COIL chemistry mechanism and 4.0×10^{-9} sec for the simulation using the 13 species, 52 reaction chemistry model. These time steps are somewhat lower than the time step of 1.0×10^{-8} sec previously reported in these investigations, and were experimentally determined by reducing the time step until stable execution was obtained. The computation was advanced to a physical time of 0.00014 sec with 143,800 time steps in the 10 species, 22 reaction simulations, and 0.00064 sec with 159,500 time steps in the 13 species, 52 reaction simulations. The physical times provide sufficient temporal advancement of the computations to address the characteristics of the predicted flow unsteadiness. The computational grid used for the COIL simulations consists of 29 blocks and 8.1 million grid cells. The computational domain which this grid discretizes represents the smallest geometrically similar element within the COIL experiment flowfield hardware, denoted a 'unit-domain.' The unit-domain consists of a supersonic (M~2.2) converging-diverging nozzle section with one large and two small injector orifices that issue

reactants into the primary flow passing through this nozzle. It was previously shown[4] that this particular configuration of the 'unit-domain', as opposed to one half as wide, splitting the large injector orifice is necessary to properly capture unsteady fluctuations in the lateral or Z direction relative to Figure 1. Figure 1 illustrates the unit-domain computational grid within the context of a surface rendering of the experiment's mixing nozzle. The orifices introduce a sonic mixture of He and I_2 into the subsonic primary flow composed of He, $O_2(^1\Delta)$, $O_2(^3\Sigma)$, H_2O, and Cl_2 inducing complex, time dependent, 3D flow structure as the jet interacts with the crossflow. It is the combination of the interfacial area created by the complex flow structure and molecular diffusion that mixes the two flows. Boundary conditions accomplish the unit-domain approximation through the enforcement of planar symmetry at the nozzle centerline in the vertical direction and with periodic surfaces on the side boundaries in the lateral direction that allow fluxes from one surface to pass through its' opposite boundary and vice-versa. No-slip constant temperature boundary conditions are used at the wetted surfaces of the nozzle and orifices, with the temperature fixed at 400K at the orifice region walls and 300K at the nozzle walls. The nozzle and injector subsonic inflow boundary conditions fix the total pressure, total temperature, and the species fractions at constant values, while the derivative of the static pressure is set to 0. The nozzle outflow boundary condition sets the second derivative of the dependent variables to 0 as is appropriate for supersonic flows.

The time accurate execution of the GASP COIL model generated a prediction of flow unsteadiness that did not decay over the time intervals where the computations were advanced, although indefinite advancement to check for decay is not an option due to the computational cost. The unsteadiness was found to extend from the jet/primary interaction region at the location of the He/I_2 transverse injection and continue downstream undiminished. Figure 2 illustrates the resulting impact of the flow unsteadiness upon the structure of the flow within the He/I_2 jet. Here an isosurface of 0.085 constant total iodine mass fraction ($I_2+I_2^*+I+I^*$) is plotted within 3D space. The surface demonstrates the presence of complex, periodic structures associated with unsteady vortex generation, and indicates strong interaction between the fluid from the large and small orifices. The break-up of the fluid from the jets occurs as the fluid from the small orifices begins to interact with that from the large, illustrated by the change in the surface from a smooth structure marked by periodic fluctuations to the more complex structure associated with the break-up. Since molecular diffusion across these surfaces and chemical reaction are strongly correlated with spatial gradients of reactant concentration, the presence of these unsteady flow structures is expected to have considerable

impact upon the predicted generation and variation of I and I*. The laser gain is directly proportional to the concentrations of I and I* and will therefore vary in a manner that follows the flow structure. This direct connection between gain and the flow structure is illustrated in Figure 3.

The underlying source of the flow unsteadiness is the presence of 'wake vortices' in the flow behind the He/I_2 jets. These vortices have their origin in the primary flow boundary layer fluid that wraps around the flow from the orifice and projects down from the wall with rotation, interacting with the fluid from the orifice. Figure 4 illustrates this process with plots of streamlines originated in the boundary layer fluid upstream of the jet in conjunction with vortex cores. The cores were extracted using the vortex core identification functions of Sujudi and Haimes[5] implemented in the Tecplot visualization software from Amtec Engineering. The red vortex core traces can be found at the center of the swirls in the streamlines, identifying the presence of vortices. Two wake vortices are seen projecting downward from the wall immediately behind the large orifice, and a third projects downward from the wall in the center of the domain between the large and small injector orifices. Additional vortices are seen projecting downward from the wall behind the small injector orifices. Fourier analysis of the flow fluctuations from the 10 species, 22 reaction simulation yielded frequencies of 56, 94, 131, and 150 kHz. The 13 species, 52 reaction simulation yielded frequencies of 12.1, 24.9, 42.3, 60.4, 96.6, 133.9, 151, and 292 kHz. The peak fluctuation amplitudes for the lateral velocities are 175 m/sec in both simulations. The predicted presence of the unsteady fluctuations within the jet structure is entirely consistent with the experimental literature on jet-in-crossflow interactions. In particular, the capture of the wake vortices as well as their location closely matches the experimental investigations.

The objective of this aspect of the investigation is to capture the fluctuations and quantify the impact on the predicted Voigt lineshape of the I $^2P_{1/2}\rightarrow^2P_{3/2}$ transition that manifests directly in the predicted gain. The vortices associated with the jet unsteadiness will rotate in a manner such that the axis of rotation is orthogonal to the optical (Z) axis. Figure 5 shows vertical and lateral plane cuts through the domain of the 13 species, 52 reaction COIL simulation, providing an illustration of some of these vortices. The scale of the vortices is such that large fractions of the gas will contribute to Doppler broadening of the transition lineshape. The optical (Z) axis or lateral velocity component W influences the Voigt function for the transition lineshape through a Doppler shift of the frequency. Figures 6 and 7 illustrate the spatial variation of the W velocity and fractional decrease in the gain within the exit plane at a single point in time from the 10

species, 22 reaction simulation; the exit plane was chosen as this location is closest to the laser cavity where gain is most important. The correlation between the spatial variation in the W velocity and the fractional gain decrease is clearly illustrated within these figures as local increases in the W velocity magnitude lead to local deceases in the line center gain.

A central question to be answered here is what effect does the unsteady flow structure have upon the lineshape predicted by the simulation? This question is answered by accumulating a dataset containing the spatial and temporal variation of the quantities necessary to calculate the gain and its' lineshape. This dataset is then spatially integrated and averaged along the Z axis in the same manner that the laser radiation passes through the device accumulating the wave of photons. This spatially averaged dataset is then temporally averaged to approximate the action of a tunable diode small signal gain probe or the lasing process over a period of time. Mathematically, this is expressed as:

$$\alpha_{ave}(\nu, y) = \frac{1}{t_{tot} z_{tot}} \iint \alpha(\nu, y, z, t) \, dz \, dt \qquad (6)$$

where t_{tot} is the total time interval of the integration, z_{tot} is the total distance of integration in the Z axis direction, and $\alpha(\nu, y, z, t)$ is laser gain prediction including the transition lineshape. For the simulations performed here, the exit plane as illustrated in Figures 6 and 7 was exported every 1.0e-07 sec of physical time, and Z integration was performed along lines of constant Y. Figures 8 and 9 show composite gain lineshapes versus normalized frequency in the exit plane for the 10 species, 13 reaction and 13 species, 52 reaction COIL simulations, where the frequency axis was normalized to let the line center of the I $^2P_{1/2} \rightarrow {}^2P_{3/2}$ transition at $1.31527 \mu m$ to be set to zero. Here, t_{tot} is $1.4 \cdot 10^{-04}$ sec for the 10 species, 22 reaction simulation and $6.4 \cdot 10^{-04}$ sec for the 13 species, 52 reaction simulation and z_{tot} is the full dimension in the z direction. The impact of the velocity component W upon the lineshape is shown in these plots. The lineshape including the influence of the gas velocity is broadened somewhat and the line center gain is lower than the line shape without it, indicating lower amplification for the regions of the flowfield where the broadening effects of the velocity field are significant.

The transition lineshapes provide additional information beyond the laser gain, however. In COIL experiments the lineshapes are analyzed to determine the gas temperature, but assume no rotation of the bulk gas flow through vortices. In this analysis, the Voigt function which describes the lineshape of the I atom transition in COILs is fit to the measured lineshape using a least-squares procedure. As the Voigt function is a convolution of Gaussian (Doppler) and Lorentzian functions and the full-width half maximum of each is proportional to the gas temperature, the temperature of the gas can be estimated with this fit. The degree to which the temperatures for the Gaussian and Lorentzian components are self-consistent is an indicator to the underlying assumptions of the fit. As shown above in Figures 8 and 9, the effect of the eddies within the flow over large periods of time relative to the characteristic timescales of fluctuation is to symmetrically broaden the lineshape, and could be misconstrued to be the result of the gas temperature. Figures 10 and 11 show temperatures extracted from the predicted lineshapes in Figures 8 and 9 compared with the Z averaged gas temperature from the solution of the conservation equations by the simulation. Comparing the lineshape temperatures from the Doppler and Lorentzian components with the thermodynamic temperature, the Doppler temperature diverges from the Lorentzian and thermodynamic temperatures in the flow regions closer to the nozzle centerline, with maximum difference being 17K. This trend is consistent with the observation that the strongest eddies tend to be more toward the center of the nozzle as illustrated in Figures 2 and 5. The Doppler temperature is clearly registering the influence of the bulk gas velocity, whereas the Lorentzian temperature remains consistent with the thermodynamic temperature. Thus, the assumption that flow rotation is negligible in the estimation of temperature from the lineshape is incorrect.

Given these results, from a theoretical standpoint it is possible to estimate the degree of flow rotation spectroscopically through the difference in the Doppler and Lorentzian temperatures. Additionally, this finding in part explains the result that experimentally determined lineshape temperatures are often on the order of 50K higher than simulation temperatures; although the 17K effect of the flow eddies found here is probably under-predicted due to vortex dissipation in the grid expansion downstream of the nozzle throat. A more detailed discussion of this work may be found with Madden[6].

A second aspect of this investigation is directed toward the development of alternative mixing nozzle concepts utilizing the knowledge gained regarding the impact of the flow unsteadiness upon the laser radiation to gas interaction and the underlying sources of the unsteadiness. As a starting point, a mixing nozzle utilizing non-reacting, supersonic injection of a He/I_2 mixture into the supersonic region of a He/O_2 primary flow was investigated both experimentally and computationally as a potential mechanism for improving laser efficiencies and increasing pressure recovery. The simulation utilized 13 blocks and 51.2 million grid cells to achieve an orthogonal grid structure. The pressure, temperature, and mass flow rates of the simulation were set to those used in the experiment. The boundary conditions used here are the same as those used above with the exception being that the entire nozzle including

lower and side walls are included in the computational domain and these surfaces were treated as no-slip boundaries. The simulation was executed with a $1 \cdot 10^{-08}$ sec timestep and time accurate integration.

A corollary to this investigation is the development of a model utilizing the simulation data that solves the ordinary differential equations describing the laser induced fluorescence of I_2, including photon production in the presence of temperature and density variations in the gas. This model provides a mechanism for direct comparison between planar laser induced fluorescence (PLIF) images from the experiment and the simulation data. Additional detail regarding this model and its' application may be found in Madden, et al.[7].

Figure 12 illustrates the predicted jet structure from the simulation through a constant I_2 mass fraction isosurface with a representation of the 600 μm PLIF laser sheet included for reference. The simulation data is interpolated onto a grid contained within this sheet to simplify the execution of the I_2 fluorescence model. The PLIF image for the experiment is compared to the simulation data using the I_2 fluorescence model in Figure 13. The comparison between the two images is very good, with the primary and secondary structures of the jet found in the PLIF image clearly shown in the simulation image. Structures not found in either image are the large scale vortices found in the previous simulations using subsonic injection. Streamtrace analysis of this injector configuration indicates that the wake vortices which contribute directly to the flow unsteadiness in subsonic injection do not have a strong interaction with the jet as in the case of subsonic injection. In order to mimic the strong wake vortex interaction, small diameter secondary injector orifices were placed behind the primary jet at varying distances. The results of these simulations are shown in Figures 14 and 15. As can be seen, no large scale vortex generation occurred in either of these cases, but increased penetration did occur which achieves the desired effect of increased mixing between the primary and secondary jets.

Parallel execution performance for GASP code on the IBM p655, the Linux Networkx Evolocity II, and the Cray XT3 supercomputer(s) is shown in Figure 13. Parallel execution speedup is 80% or above through 960 processors and is at 65% at 1,600 processors. The communications costs are directly attributable to the use of fully implicit integration, requiring communication of zonal boundary information after an inner iteration of the Gauss-Seidel matrix inversion solver. Communications costs increase with the number of variables tracked reflected in this work in the number of species used in the COIL chemistry mechanism. Increasing the number of variables increases the amount of data transmitted during each communications pass, and thus increases the fraction of time that communications occupy the overall computation time. Also, increasing the number of iterations on the inner problem increased the number of data exchanges between processors per timestep, thereby increasing the communications costs. As is typical with the domain decomposition model used by GASP for parallel execution, memory use decreases as the number of processors used increases.

4. Summary

In conclusion, the simulations explored here illustrate various aspects of chemical laser simulation. The unsteady COIL simulations provided here predict that bulk gas flow velocity components associated with vortex rotation will broaden the lineshape of quantum transitions of the species within the gas flow. These simulations demonstrate that if the bulk gas velocity influence is ignored when fitting spectral functions to the lineshape and these vortices are present, the temperature extracted will be higher than the actual temperature. The results found here indicate that this difference may be as high as 17K, but even this prediction may be low due to under-prediction of vortex strength associated with numerical dissipation. It is suggested that the difference between the Doppler and Lorentzian temperatures extracted from the spectral lineshape fit could be correlated against changes in fluid dynamic parameters such as Reynolds number to determine trends as well as the magnitude of flow rotation.

Additionally, a model for laser-induced fluorescence of I_2 was developed as a tool to directly compare simulation data with experiment flow imaging diagnostics. A comparison between the experiment and simulation images for a new mixing nozzle concept, showed very good agreement. This imagery in combination with additional analysis of the simulation data was used to further develop the mixing nozzle by the addition of secondary injector orifices for the purpose of enhancing the mixing. Simulations of these new mixing nozzle concepts indicated that while the goal of inducing flow unsteadiness was not reached, the penetration of the jet was increased and did provide some degree of mixing enhancement. Further simulations will be performed to ascertain the performance of these concepts from the COIL operation standpoint.

References

1. Perram, G.P, *Int. J. Chem: Kinet.*, 27, pp. 817–28, 1995.

2. Madden, T.J. and W. C. Solomon, *AIAA 97-2387*, 28th Plasmadyamics and Lasers Conference, Atlanta, GA, June 23–25, 1997.

3. Madden, T.J., *SPIE Proceedings of XIV International Symposium On Gas Flow & Chemical Lasers and High Power Laser Conference*, Wrocław, Poland, 25–30 August, 2002.

4. Madden, T.J. "An Analysis of Mechanisms Underlying Flow Unsteadiness in Chemical Oxygen-Iodine Laser Mixing Systems." *AIAA-2005-5390*, 36th AIAA Plasmadynamics and Lasers Conference, Toronto, Ontario, Canada, June 6–9, 2005.

5. Sujudi, D. and R. Haimes, "Identification of Swirling Flow in 3-D Vector Fields." *AIAA Paper 95-1715*, 12th AIAA Computational Fluid Dynamics Conference and Open Forum, San Diego CA, 19–22 June 1995.

6. Madden, T.J. "The Influence of Flow Unsteadiness upon the Estimation of Temperature from the I $^2P_{1/2} \rightarrow ^2P3/_2$ Transition Lineshape."38th AIAA Plasmadynamics and Lasers Conference, Miami, FL, 25–28 June, 2007.

7. Madden, T.J., C.A., Noren, L. Emmert, and M. Heaven, "A Model for the Prediction of I_2 Fluorescence in the Presence of Pulsed Laser Radiation utilizing Computational Fluid Dynamic Simulation Datasets." 38th AIAA Plasmadynamics and Lasers Conference, Miami, FL, 25–28 June, 2007.

Figure 2. A snap shot in time of unsteady fluid dynamic structures manifested in the He/I_2 jet from the 'first principals' 3D GASP COIL simulations. A surface of constant total iodine mass fraction, value = 0.085, acts as a scalar tracer for the jet structure.
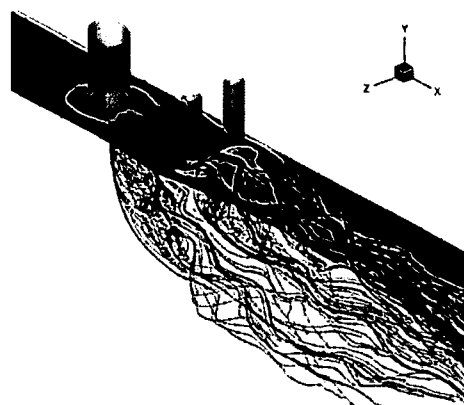

Figure 1. Computational grid used in the 3D GASP COIL simulations, shown in relation to a rendering of the wetted surfaces in the COIL laser hardware. This grid also presents the geometric similarity used to simplify the much larger physical domain into a realistic computational domain, denoted the unit-domain.

FiFgure 4. 3D streamtraces (in black) initiated upstream of the large injector orifice at 2% of the channel height from the wall in conjunction with vortex cores (in red) extracted from the 10 species, 22 reaction 3D GASP COIL simulations
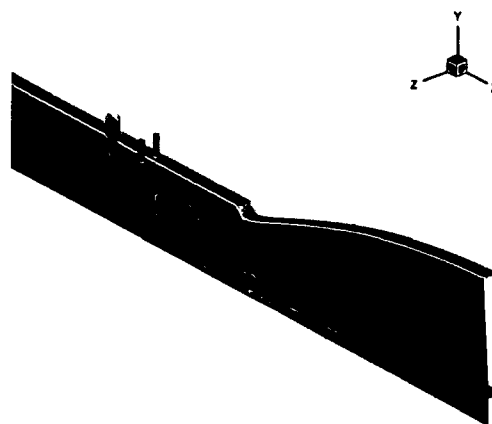

Fgure 3. A snap shot in time of an isosurface of constant gain, value = 0.3 %/cm, from the 10 species, 22 reaction 3D GASP COIL simulations illustrating the explicit dependence of laser gain on flow structure

Figure 5. I_2 mole fraction distribution within 2D. planes in the 8 million grid cell, 13 species, 52 reaction COIL hardware simulations illustrating flow structure and fluctuation structure
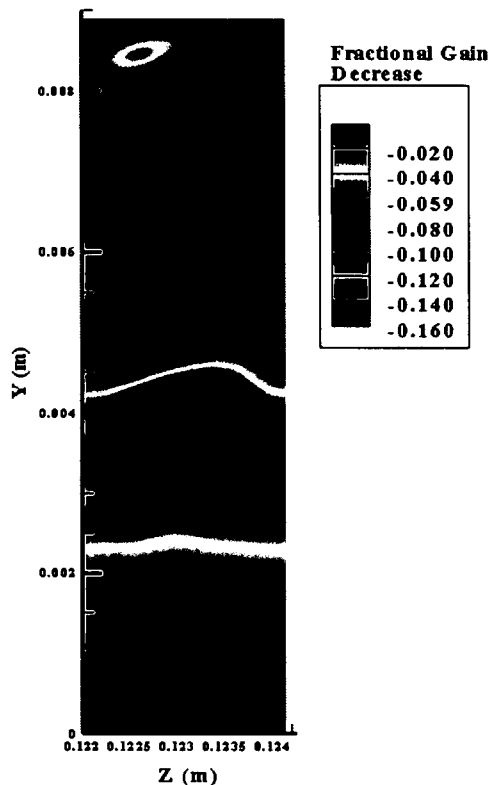
163

Figure 7. Fractional decrease in the gain calculation due to the *W* velocity component for a time slice in the exit plane of the 13 species, 52 reaction simulations
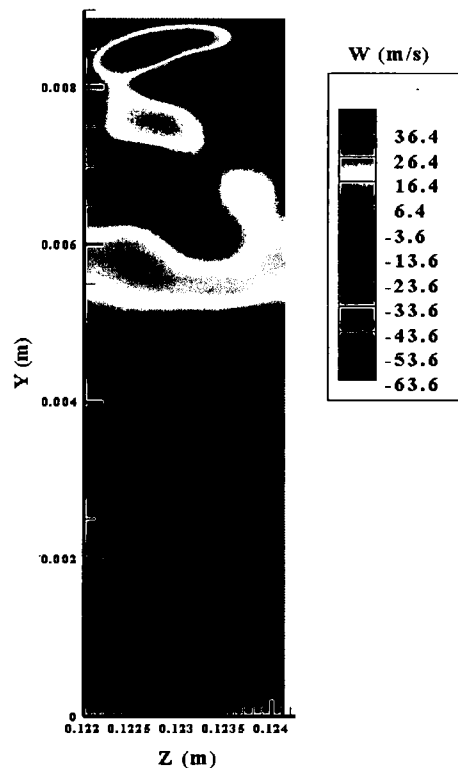

Figure 6. Time slice of *W* velocity component within the exit plane of the 13 species, 52 reaction simulations
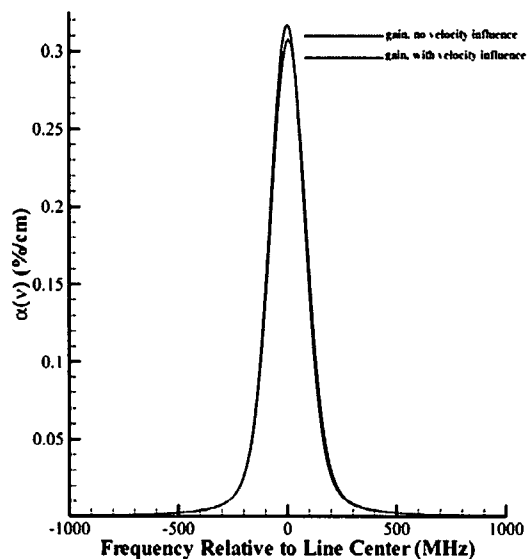

Figure 8. Time, space averaged gain lineshape from the 8 million grid cell, 10 species, 22 reaction COIL simulations
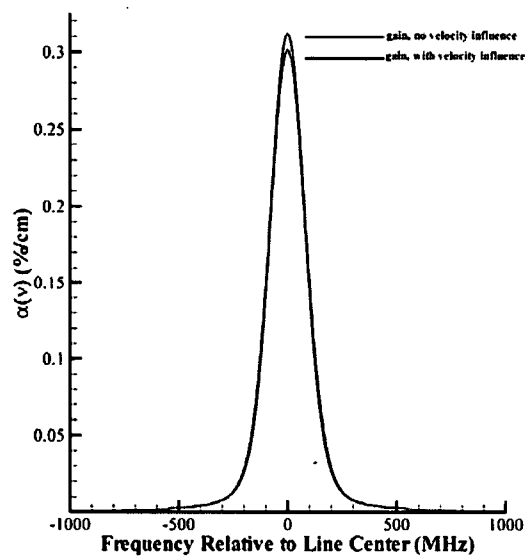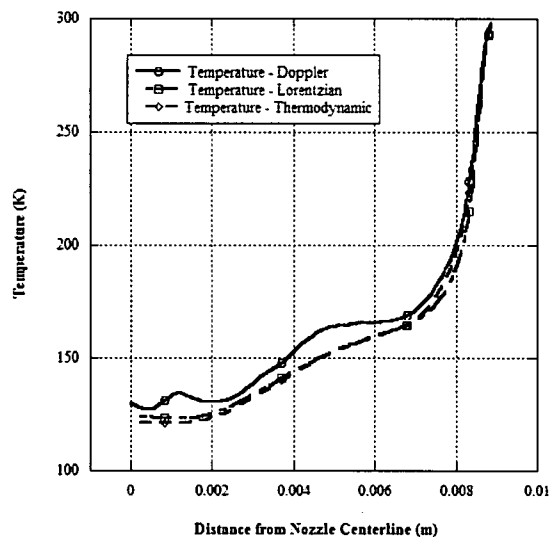

Figure 9. Time, space averaged gain lineshape from the 8 million grid cell, 13 species, 52 reaction COIL simulations

Figure 11. Comparison of temperature values from the 13 species, 52 reaction simulation; Doppler and Lorentzian values were determined based upon the lineshape in Figure 9. The thermodynamic temperature is averaged from the simulation data.
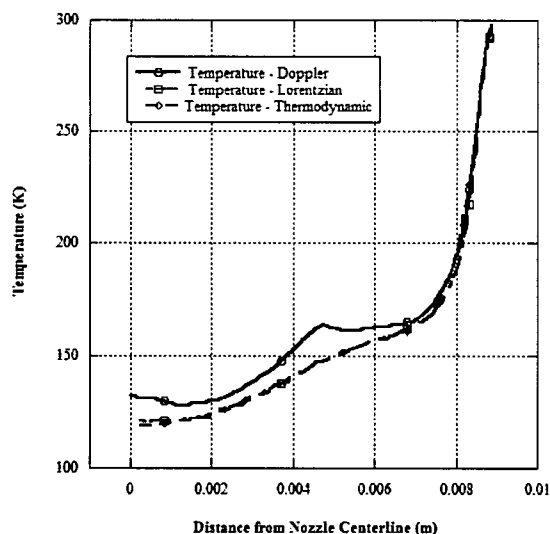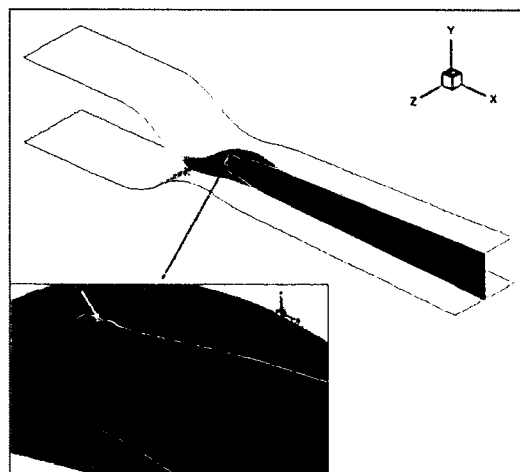

Figure 10. Comparison of temperature values from the 10 species, 22 reaction simulation; Doppler and Lorentzian temperatures were determined based upon the lineshape in Figure 8. The thermodynamic temperature is averaged from the simulation data.

Figure 12. Illustration of 'sheet' sub-domain used for execution of the I_2 fluorescence model, in blue, with respect to the larger computational domain used in the 3-D Navier-Stokes simulation. Values are interpolated from the Navier-Stokes simulation domain to the 'sheet' domain.
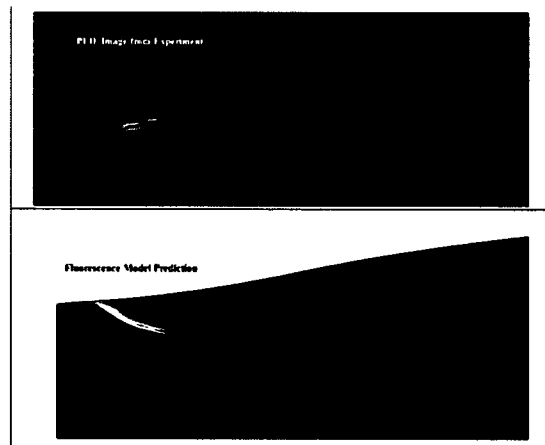

Figure 13. Comparison of an experiment PLIF image with an I_2 fluorescence model generated image within the streamwise laser sheet shown in Figure 12
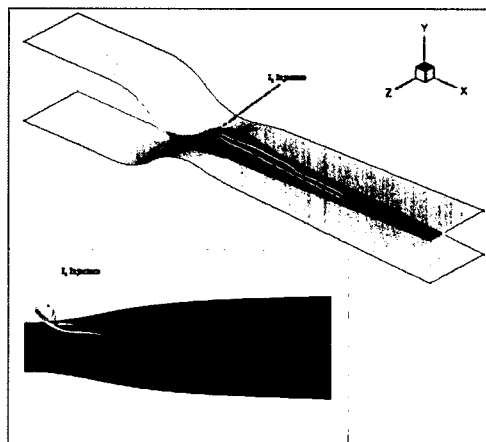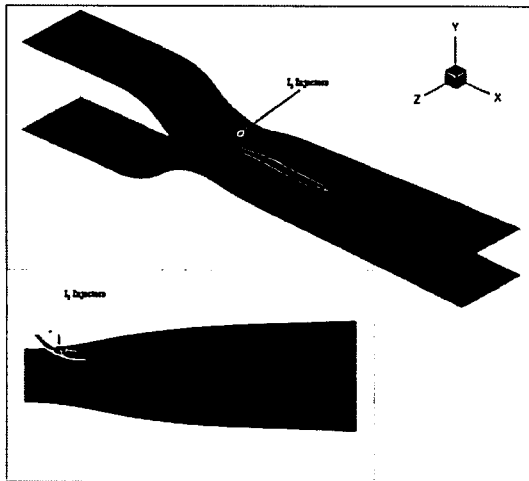

Figure 15. I_2 isosurface and contour plot for a new mixing nozzle concept utilizing supersonic injection of I_2. Note that the second injector is ½ the distance to the primary injector of that used in the simulation shown in Figure 14.

165

Figure 14. I_2 isosurface and contour plot for a new mixing nozzle concept utilizing supersonic injection of I_2. Note that a second injector is used to modify the mixing characteristics of the primary injector.
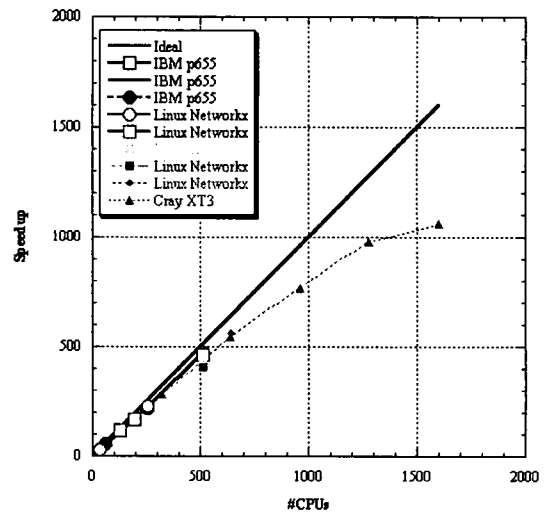

Figure 16. Speedups for GASP on the IBM p655, Linux Networkx cluster, and Cray XT3 for varying number of species and processors. Note that the XT3 data is for a simulation using 13 species, thereby increasing the communications costs by a factor of 2.5 over a single gas simulation.

166